Type-0 second order nonlinear interaction in monolithic waveguides of isotropic semiconductors

Payam Abolghasem, Junbo Han, Bhavin J. Bijlani, and Amr S. Helmy*

The Edward S. Rogers Sr. Department of Electrical and Computer Engineering, University of Toronto, 10 King's College Road, Toronto, Ontario M5S 3G4, Canada

*a.helmy@utoronto.ca

http://photonics.light.utoronto.ca/helmy/

Abstract: We report the observation of type-0 phase-matching in bulk *z*-grown $Al_xGa_{1-x}As$ Bragg reflection waveguides where TM-polarized second-harmonic is generated using TM-polarized pump. For a pulsed pump with 1.8 ps temporal width and an average power of 3.3 mW, second-harmonic power of 16 μW was detected at 1567.8 nm. The normalized nonlinear conversion efficiency was obtained to be 2.84×10^3 $\%W^{-1}cm^{-2}$ in a 2.2 mm long waveguide. The highly versatile modal birefringence in Bragg reflection waveguides enabled the phase-matching of the three modalities; namely type-0 $TM_\omega \rightarrow TM_{2\omega}$, type-I $TE_\omega \rightarrow TM_{2\omega}$ and type-II $TE_\omega + TM_\omega \rightarrow TE_{2\omega}$ interactions to simultaneously take place within a spectral bandwidth as small as 17 nm.

OCIS codes: (190.2620) Harmonic generation and mixing; (190.4390) Nonlinear optics, integrated optics.

References and links

1. Y. Shih, "Entangled biphoton source-property and preparation," Rep. Prog. Phys. **66**, 1009 (2003).
2. C. K. Hong, Z. Y. Ou, and L. Mandel, "Measurement of subpicosecond time intervals between 2 photons by interference," Phys. Rev. Lett. **59**, 2044–2046 (1987).
3. I. Shoji, T. Kondo, A. Kitamoto, M. Shirane, and R. Ito, "Absolute scale of second-order nonlinear optical coefficients," J. Opt. Soc. Am. B **14**, 2268–2294 (1997).
4. E. D. Palik, *Handbook of Optical Constants of Solids* (Academic Prsee, Orlando, Florida, 1985).
5. M. Ravaro, M. Le Dû, J. P. Likforman, S. Ducci, V. Berger, G. Leo, and X. Marcadet, "Estimation of parametric grain in GaAs/AlO_x waveguides by fluorescence and second harmonic generation measurements," Appl. Phys. Lett. **91**, 191119 (2007).
6. X. Yu, L. Scaccabarozzi, J. S. Harris, P. S. Kuo, M. M. Fejer, "Efficient continuous wave second harmonic generation pumped at 1.55 μm in quasi-phase-matched AlGaAs waveguides," Opt. Express **13**, 10742–10748 (2005).
7. B. R. West and A. S. Helmy, "Analysis and design equations for phase matching using Bragg reflection waveguides," IEEE J. Quantum Electron. **12**, 431–442 (2006).
8. P. Abolghasem, J. Han, A. Arjmand, B. J. Bijlani, and A. S. Helmy, "Highly efficient second-harmonic generation in monolithic matching-layer enhanced $Al_xGa_{1-x}As$ Bragg reflection waveguides," IEEE Photon. Technol. Lett. **21**, 1462–1464 (2009).
9. J. S. Aitchison, M. W. Street, N. D. Whitbread, D. C. Hutchings, J. H. Marsh, G. T. Kennedy, and W. Sibbet, "Modulation of the second-order nonlinear tensor components in multiple-quantum-well structures," IEEE Sel. Top. Quantum Electron. **4**, 695–700 (1998).
10. J. P. Bouchard, M. Tetu, S. Janz, D. X. Xu, Z. R. Wasilewski, P. Piva, U. G. Akano, and I. V. Mitchell, "Quasi-phase matched second-harmonic generation in an AlxGa1-xAs asymmetric quantum-well waveguide using ion-implantation-enhanced intermixing," Appl. Phys. Lett. **77**, 4247–4249 (2000).

#124649 - $15.00 USD Received 24 Feb 2010; revised 23 May 2010; accepted 26 May 2010; published 28 May 2010

11. P. N. Butcher and D. Cotter, *The Elements of Nonlinear Optics* (Cambridge University, Cambridge, UK. 1990).
12. Lumerical Solutions, www.lumerical.com.
13. S. Gehrsitz, F. K. Reinhart, C. Gourgon, N. Herres, A. Vonlanthen, and H. Sigg, "The refractive index of Al_xGa1_xAs below the band gap: Accurate determination and empirical modeling," Appl. Phys. **87**, 7825–7837 (2000).
14. B. R. West and A. S. Helmy, "Analysis and design equations for phase matching using Bragg reflection waveguides," IEEE J. Quantum Electron. **12**, 431–442 (2006).
15. K. Moutzouris, S. V. Rao, M. Ebrahimzadeh, A. De Rossi, V. Berger, M. Calligaro, V. Ortiz, "Efficient second-harmonic generation in birefringently phase-matched $GaAs/Al_2O_3$ waveguides," Opt. Lett. **26**, 1785–1787 (2001).

1. Introduction

Second-order optical nonlinearities play a key role in numerous applications. These include both established and emerging fields such as optical-frequency converters, optical parametric oscillators (OPOs), photon-pair sources [1] and quantum interferometers [2]. Compound semiconductors represent an important class of materials that provides an excellent platform to utilize second-order nonlinear optical processes. For example $GaAs/Al_xGa_{1-x}As$ benefits from large $\chi^{(2)}$ nonlinearity ($d_{14}^{GaAs} \approx 119$ pm/V around 1550 nm) [3], broad transparency window ($0.9-17\ \mu$m), excellent thermal conductivity [4] and well developed fabrication technology. However, the cubic structure ($\bar{4}3m$ symmetry) of $GaAs/Al_xGa_{1-x}As$ renders these crystals optically isotropic and lack of intrinsic birefringence. As a result, phase-matching (PM) $\chi^{(2)}$ nonlinearities involves significant challenges in these crystals. Several techniques have been developed so far for phase-matching bulk nonlinear coefficients, of $GaAs/Al_xGa_{1-x}As$. Artificial birefringence [5] and quasi-phase-matching [6] have been the most successful methods to date. Another technique uses Bragg reflection waveguides (BRWs), where the strong modal dispersion properties of 1-dimensional photonic bandgap structures are used to attain exact phase-matching [7, 8].

For photonics applications, the $GaAs/Al_xGa_{1-x}As$ system is grown along the $[001]$ crystal axis with $[\bar{1}10]$ cleavage planes. Two types of nonlinear interactions arise from the non-vanishing susceptibility tensor elements; namely type-I interaction where a TE_ω-polarized pump (FH) generates $TM_{2\omega}$-polarized second-harmonic (SH) and type-II interaction where a pump with hybrid TE_ω+TM_ω polarization state generates $TE_{2\omega}$-polarized SH. Type-II is known to be more efficient as it benefits from enhanced effective second-order nonlinearity. Beside the relative efficiency of the aforementioned interactions, their polarization selection rules govern the applications within which they are used. For instance, in generating frequency entangled photon-pairs in a spontaneous parametric down-conversion process (SPDC), the phase-matching type governs the polarization state of the down-converted photons. Adding other types of interactions to the existing ones $TE_\omega \rightarrow TM_{2\omega}$ and TE_ω+$TM_\omega \rightarrow TE_{2\omega}$ would further enrich the capabilities and functionality obtained by using the $\chi^{(2)}$ nonlinearity of the $GaAs/Al_xGa_{1-x}As$ system in classical and non-classical applications.

2. Theoretical Background

In this work, we demonstrate the modality of type-0 second order nonlinear interaction in isotropic semiconductor waveguides; namely Bragg reflection waveguides. Here, a TM_ω-polarized pump is used to generate second-harmonic with $TM_{2\omega}$ polarization state. The $TM_\omega \rightarrow TM_{2\omega}$ interaction has been previously reported in asymmetric multiple-quantum-well waveguides, where the broken symmetry of the structure along the z-axis induced a weak susceptibility tensor element $\chi_{zzz}^{(2)}$ [9, 10]. In the structure discussed here, isotropic semiconductors were utilized. The source of $TM_\omega \rightarrow TM_{2\omega}$ interaction is not due to the appearance of $\chi_{zzz}^{(2)}$ element. Rather; it is ascribed to the characteristic of TM_ω propagating mode where the pump elec-

#124649 - $15.00 USD Received 24 Feb 2010; revised 23 May 2010; accepted 26 May 2010; published 28 May 2010

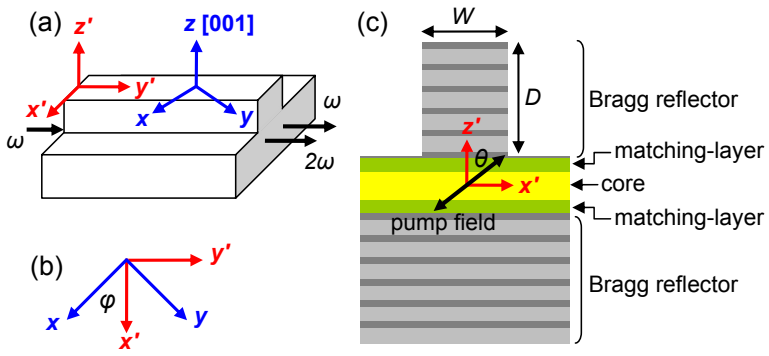

Fig. 1. (a) Schematic of waveguide where $x'y'z'$ and xyz indicating the laboratory and crystal frames, respectively. (b) Orientation of the reference frames with an orientation angle of $\phi = \pi/4$. (c) Schematic of the cross section of the characterized matching-layer enhanced BRW [8] with the ridge width of $W = 4.4\ \mu$m and the ridge depth of $D = 3.6\ \mu$m. For type-0 $TM_\omega \rightarrow TM_{2\omega}$, type-I $TE_\omega \rightarrow TM_{2\omega}$ and type-II $TE_\omega + TM_\omega \rightarrow TE_{2\omega}$ interactions the angle between the electric field of the incident pump beam with [001] crystal axis is $\theta = 0, \pi/4$ and $\pi/2$, respectively.

tric field has a non-zero component along the propagation direction. It is further demonstrated that the observed $TM_\omega \rightarrow TM_{2\omega}$ interaction can simultaneously take place with $TE_\omega \rightarrow TM_{2\omega}$ and $TE_\omega + TM_\omega \rightarrow TE_{2\omega}$ processes within a narrow spectral range and with comparable efficiency. This in turn allows one to utilize all three interactions provided that the phase-matching wavelengths of all three processes reside within the pump spectral bandwidth; a condition that can be easily met by using femtosecond pulses. This unique characteristic is enabled by the versatile, tunable modal birefringence of $TE_{2\omega}$ and $TM_{2\omega}$ Bragg modes in BRWs with quarter-wave periodic claddings, which can be controlled while maintaining PM. Making available the new modality of type-0 nonlinear interaction in this class of materials would have significant scientific and practical ramifications; it further enhance the efficiency of frequency conversion and can also provide a new degree of freedom for entangled photon-pair generation.

In order to understand the origin of this newly observed $TM_\omega \rightarrow TM_{2\omega}$ interaction, light needs to be shed on second order nonlinear interactions in $Al_xGa_{1-x}As$ semiconductors. In bulk $Al_xGa_{1-x}As$ waveguides, second order nonlinear interactions rely on accessing the nonlinear tensor element $\chi^{(2)}_{xyz}$. Customarily, this is achieved in waveguides with [001] fabrication growth direction and [110] cleaved facets. A schematic of a representative matching-layer enhanced BRW [8] used in this study is shown in Fig. 1. The coordinate systems xyz and $x'y'z'$, in Fig. 1(a), denote the crystal and laboratory frames respectively. The two reference frames are rotated by an angle of $\phi = \pi/4$ with respect to the crystal z-axis [see Fig. 1(b)]. For simplicity, the analysis is performed in the $x'y'z'$ coordinates, where the major fields of TE and TM propagating modes are aligned with the axes of the reference frame. It is further assumed that the scalar wave equations are justified in expressing the propagation of the optical modes. The modal electric field at ω_σ frequency, $\omega_\sigma \in \{\omega, 2\omega\}$, can be written as:

$$E^{\mu'}_{\omega_\sigma}(x',y',z') = A_{\omega_\sigma}(y') E^{\mu'}_{\omega_\sigma}(x',z') \exp(ik_{\omega_\sigma} y') \tag{1}$$

where $\mu' \in \{x',y',z'\}$, A_{ω_σ} is the slowly varying amplitude, $E^{\mu'}_{\omega_\sigma}(x',y')$ is the normalized spatial profile and k_{ω_σ} is the propagation constant. The μ'-th component of the second-order electric

#124649 - $15.00 USD Received 24 Feb 2010; revised 23 May 2010; accepted 26 May 2010; published 28 May 2010

polarization vector at 2ω writes [11]:

$$[P^{(2)}_{2\omega}]_{\mu'} = \varepsilon_0 K \chi^{(2)}_{\mu'\alpha'\beta'} E^{\alpha'}_{\omega} E^{\beta'}_{\omega} \tag{2}$$

where $\{\alpha',\beta'\} \in \{x',y',z'\}$ and K is the degeneracy factor, which is equal to $1/2$ for second-harmonic generation (SHG). The elements of the susceptibility tensor in the laboratory and crystal frames are related to each other using the transformation [11]:

$$\chi^{(2)}_{\mu'\alpha'\beta'} = R_{\mu'\mu}(\phi) R_{\alpha'\alpha}(\phi) R_{\beta'\beta}(\phi) \chi^{(2)}_{\mu\alpha\beta} \tag{3}$$

where $R_{j'j}(\phi)$ are the elements of the rotation matrix with the rotation angle of $\phi = \pi/4$. Using Eq. (3), the non-zero elements of $\chi^{(2)}$ tensor in the $x'y'z'$ frame are:

$$\chi^{(2)}_{x'x'z'} = \chi^{(2)}_{x'z'x'} = \chi^{(2)}_{z'x'z'} = +\chi^{(2)}_{xyz} \tag{4a}$$

$$\chi^{(2)}_{y'y'z'} = \chi^{(2)}_{y'z'y'} = \chi^{(2)}_{z'y'y'} = -\chi^{(2)}_{xyz} \tag{4b}$$

Unlike in the crystal frame where $\chi^{(2)}_{\mu\alpha\beta}$ is non-zero for $\mu \neq \alpha \neq \beta$, from Eq. (4), it can be seen that in the laboratory coordinate system, $\chi^{(2)}_{\mu'\alpha'\beta'}$ is non-zero for those permutations of x', y' and z' for which two indices are identical while the third index is z'.

For a pump mode with TM_ω polarization state, the major field components are $(H^{x'}_{\omega}, E^{y'}_{\omega}, E^{z'}_{\omega})$. Using Eqs. (2)–(4), the elements of the electric polarization vector in the laboratory frame are:

$$[P^{(2)}_{2\omega}]_{x'} = 0 \tag{5a}$$

$$[P^{(2)}_{2\omega}]_{y'} = -\varepsilon_0 \chi^{(2)}_{xyz} E^{z'}_{\omega} E^{y'}_{\omega} \tag{5b}$$

$$[P^{(2)}_{2\omega}]_{z'} = -\frac{\varepsilon_0}{2} \chi^{(2)}_{xyz} E^{y'}_{\omega} E^{y'}_{\omega} \tag{5c}$$

From Eq. (5), the existence of the non-vanishing electric polarization component, $[P^{(2)}_{2\omega}]_{z'}$, can support second-harmonic generation with $\mathrm{TM}_{2\omega}$ polarization state. This SH signal does not lend itself to the broken symmetry along the crystal z-axis hence the appearance of $\chi^{(2)}_{zzz}$ tensor element, rather it originates from the pump electric field component, $E^{y'}_{\omega}$, which lies along the propagation direction. In order to obtain a better understanding about the strength of the second-harmonic in type-0 interaction, it would be instructive to examine the electric field components of TM modes of both harmonics in a typical BRW. In Fig. 2, we have plotted the magnitudes of electric field components for TM_ω polarized pump $(E^{x'}_{\omega}, E^{y'}_{\omega}, E^{z'}_{\omega})$ and those for $\mathrm{TM}_{2\omega}$ polarized second-harmonic $(E^{x'}_{2\omega}, E^{y'}_{2\omega}, E^{z'}_{2\omega})$ obtained using a full-vectorial mode solver [12] for the structure reported in [8]. From the figure, it can be deduced that the magnitude of the pump electric field along the propagation direction, $E^{y'}_{\omega}$, is approximately within the same order of magnitude of that of the dominate field component $E^{z'}_{\omega}$. As such, it is to observe the generated $\mathrm{TM}_{2\omega}$ polarized SH with noticeable strength in the type-0 interaction. Also in Fig. 2, it is interesting to compare the magnitudes of the field components $E^{x'}_{\omega}$ and $E^{z'}_{\omega}$. It can be seen that $|E^{x'}_{\omega}|$ is comparable with $|E^{z'}_{\omega}|$ which can be attributed to the hybrid nature of optical modes in ridge waveguides. Unlike slab waveguides where propagating modes can be split into pure TE and pure TM modes, such decomposition in ridge structures is viable only as an approximation which is adopted for analytical simplifications. The same comparison at 2ω frequency reveals the fact that $|E^{x'}_{2\omega}|$ is almost two orders of magnitudes smaller than $|E^{z'}_{2\omega}|$. The fact that $|E^{x'}_{\omega}|$ is

#124649 - $15.00 USD Received 24 Feb 2010; revised 23 May 2010; accepted 26 May 2010; published 28 May 2010

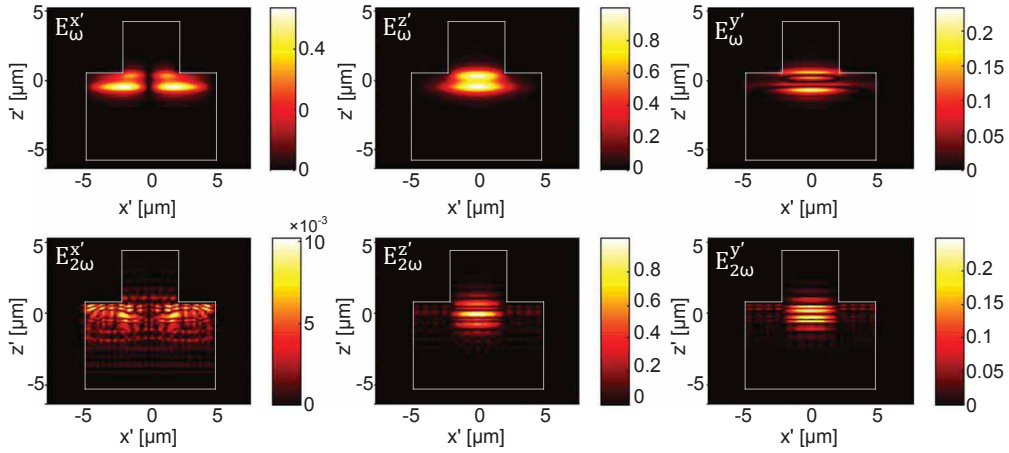

Fig. 2. Simulated magnitudes of electric field components [V/m] for TM_ω propagating pump at ω frequency $(E_\omega^{x'}, E_\omega^{y'}, E_\omega^{z'})$ and those for $TM_{2\omega}$ propagating second-harmonic at 2ω frequency $(E_{2\omega}^{x'}, E_{2\omega}^{y'}, E_{2\omega}^{z'})$. The fields profiles were simulated using Lumerical mode solver [12].

comparable with $|E_\omega^{z'}|$ while $|E_{2\omega}^{x'}|$ is significantly smaller than $|E_{2\omega}^{z'}|$ can be explained by the difference between the wavelengths of pump and second-harmonic with respect to the waveguide dimensions. Due to the longer wavelength at the pump frequency, the physical dimensions of the ridge which offer the lateral confinement become more comparable to the optical mode. As a result, the effect of 2-D confinement of the ridge in rendering the propagating mode polarization hybrid nature is more pronounced at the pump wavelength.

The expected smaller magnitude of generated second-harmonic in $TM_\omega \rightarrow TM_{2\omega}$ interaction may justify why type-0 process in $Al_xGa_{1-x}As$ has not received attention in the literature. However, the characterization results discussed in the next section, demonstrates that even with the existence of a small $E_\omega^{y'}$ component, a strong second-harmonic can be generated thanks to the high efficiency of the nonlinear interaction in Bragg reflection waveguides.

3. Characterization Results

The waveguide structure and its fabrication has been previously reported in [8]. The characterized device was a ridge waveguide with a ridge width of 4.4 μm and a ridge depth of 3.6 μm. The length of the device was 2.2 mm. Nonlinear characterization was carried out in an end-fire rig setup using pulses with a temporal width of 1.8 picosecond. The pulses were nearly transform limited with a temporal-spectral bandwidth product of $\Delta\tau\Delta\nu = 0.53$ and with a repetition rate of 76 MHz. Optical pulses were coupled to the waveguide using a 40× diode objective lens ($T \approx 0.98$). The emerging signal was collected using a 60× objective lens ($T \approx 0.78$). The average power of the pump was recorded using InGaAs photodetectors. Second-harmonic power was monitored using a Si photodectector. A polarization beam splitter with TM passing configuration was used after the output objective lens to examine the polarization of generated SH.

The scan of SH power as a function of pump wavelength is illustrated in Fig. 3(a). For comparison, we have also plotted the tuning curves of $TE_\omega \rightarrow TM_{2\omega}$ and $TE_\omega + TM_\omega \rightarrow TE_{2\omega}$ interactions as previously reported in [8]. For the current samples, the internal pump power (P_ω), after accounting for facet reflection (29%) and input coupling factor (49%), was estimated to be 3.3 mW, which was the same pump power used in [8]. Peak internal SH power ($P_{2\omega}$)

#124649 - $15.00 USD Received 24 Feb 2010; revised 23 May 2010; accepted 26 May 2010; published 28 May 2010

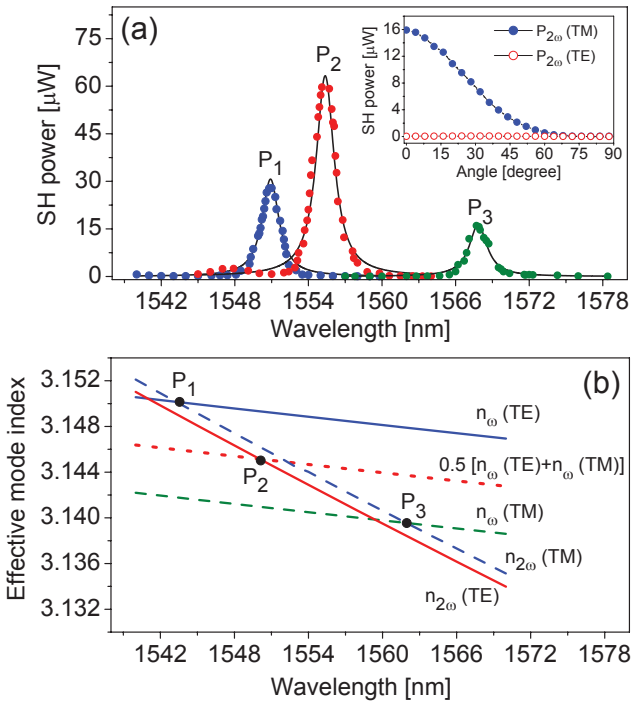

Fig. 3. (a) Second-harmonic power as a function of pump wavelength measured for three phase-matching scheme. The solid lines are the Lorentzian fit to the measured date. (Inset) Variation of $TE_{2\omega}$ and $TM_{2\omega}$ components of SH power as a function of pump angle θ at phase-matching wavelength of 1567.8 nm. (b) Simulated modal dispersion of fundamental modes of pump and SH. The crossing points P_1, P_2 and P_3 denote the phase-matching point for $TE_\omega \rightarrow TM_{2\omega}$, $TE_\omega + TM_\omega \rightarrow TE_{2\omega}$ and $TM_\omega \rightarrow TM_{2\omega}$ processes, respectively.

estimated before the end facet of the waveguide was obtained to be 16 μW at 1567.8 nm. We calculated the normalized conversion efficiency ($\eta = P_{2\omega}/P_\omega^2 L^2$) to be 2.84×10^3 %W^{-1}cm^{-2} for the sample with $L = 2.2$ mm length. The inset of Fig. 3(a) shows the variation of $TE_{2\omega}$ and $TM_{2\omega}$ components of SH power as a function of θ, the angle between the pump field and the z-axis of the crystal, when there was no polarization beam splitter at the output stage. As expected, the magnitude of $TE_{2\omega}$ component was practically zero, while the $TM_{2\omega}$ component was decreasing with the increase of θ.

The estimated value of η is noteworthy when compared with the efficiencies of type-I $TE_\omega \rightarrow TM_{2\omega}$ and type-II $TE_\omega + TM_\omega \rightarrow TE_{2\omega}$ interactions [8]. A summary of the performance of the three processes is provided in Table 1. From the table it is apparent that the efficiency of type-0 interaction is within the same order of magnitude as those of the $TE_\omega \rightarrow TM_{2\omega}$ and $TE_\omega + TM_\omega \rightarrow TE_{2\omega}$ processes. To the best of our knowledge, this unique behaviour of BRWs in simultaneously offering high efficient nonlinear interaction with additional degrees of freedom in controlling the polarization of the generated harmonic is not offered by any other waveguide structure and by any other phase-matching scheme.

We further simulated the modal dispersion of the pump and second-harmonic for both orthogonal polarizations to justify the experimental phase-matching points in Fig. 3(a). The result is shown in Fig. 3(b) where P_1, P_2 and P_3 denote the phase-matching points associated with $TE_\omega \rightarrow TM_{2\omega}$, $TE_\omega + TM_\omega \rightarrow TE_{2\omega}$ and $TM_\omega \rightarrow TM_{2\omega}$ interactions, respectively. In comparing Fig. 3(a) and 3(b), the slight mismatch of less than 7 nm between the measured phase-matching

#124649 - $15.00 USD Received 24 Feb 2010; revised 23 May 2010; accepted 26 May 2010; published 28 May 2010

Table 1. Summary of the three phase-matched second-harmonic generation

Nonlinear Process	θ [rad]	P_ω [mW]	$P_{2\omega}$ [μW]	η [%W^{-1}cm^{-2}]
Type-0: TM$_\omega$→TM$_{2\omega}$	0	3.3	16	2.84×10^3
Type-I: TE$_\omega$→TM$_{2\omega}$	$\pi/2$	3.3	28	5.30×10^3
Type-II: TE$_\omega$+TM$_\omega$→TE$_{2\omega}$	$\pi/4$	3.3	60	1.14×10^4

wavelengths and those predicted from simulation was inevitable due to inaccuracies of the refractive index model of $Al_xGa_{1-x}As$ elements [13] as well as the fabrication tolerances and imperfections.

The TM$_\omega$→TM$_{2\omega}$ interaction could also exist due to the hybrid nature of modes in 2-D guided structures. We investigated the waveguide influence on polarization coupling by examining the ratio between the TM$_\omega$ to TE$_\omega$ components of the pump power before and after the waveguide. The measurement resulted in a ratio of ≈ 100 before the input objective lens while it was ≈ 21 after the output objective lens. Such a small TE$_\omega$ component cannot be entirely accounted for initiating a type-I TE$_\omega$→TM$_{2\omega}$ interaction with the level of SH power observed here given the field ratios alone. This confirms that the observed nonlinear process was indeed type-0 TM$_\omega$→TM$_{2\omega}$ interaction.

It can be clearly seen from Figs. 3(a) and 3(b) that the phase-matching wavelengths of all three nonlinear interactions can be semi-independently tailored by waveguide design and in this case they reside within a spectral range as small as 17 nm. This spectral range lies within the spectral bandwidth of typical ultra-short pulses with temporal widths of a few hundred femtoseconds. The close proximity of the observed phase-matching wavelengths allows one to generate a second-harmonic signal with mixed polarization states. In practice, such flexibility might be potential for certain polarization sensitive applications. An example is an integrated source of photon-pairs, where controlling the polarization entanglement is the major interest. This can be carried out in SPDC processes with ultrashort pump where the pump spectral bandwidth is large enough to cover the phase-matching wavelengths of all three type-0, type-I and type-II interactions. Generating photon-pairs with different polarization-entangled states can then be carried out in a single device by simply rotating the polarization angle of the incident pump beam (the angle θ in Fig. 1). Polarization insensitive applications can also benefit from the current design. For example wideband SHG can be expected using a mixed TE$_\omega$/TM$_\omega$ polarized femtosecond pump while both polarization components of the SH are maintained.

The modal birefringence of a propagating mode at frequency ω_σ is defined as $\Delta n_{\omega_\sigma} = n_{\omega_\sigma}^{(\mathrm{TE})} - n_{\omega_\sigma}^{(\mathrm{TM})}$ where $n_{\omega_\sigma}^{(\mathrm{TE})}$ and $n_{\omega_\sigma}^{(\mathrm{TM})}$ are the effective indices of TE$_{\omega_\sigma}$ and TM$_{\omega_\sigma}$ modes. In this work, the small birefringence of the second harmonic mode played a pivotal role in obtaining the phase-matching wavelengths of all three nonlinear interactions discussed above in proximity of each other. For slab BRWs with quarter-wave Bragg mirrors, it is known that $\Delta n_{2\omega} = 0$ denoting the fact that the lowest order Bragg modes are polarization degenerate [14]. Departing from the quarter-wave condition by either imposing the lateral confinement of a ridge structure or incorporating non-quarter-wave layers in transverse Bragg reflectors (TBRs) results in polarization non-degeneracy of fundamental Bragg mode. To further clarify this in Fig. 4, we simulated the birefringence at ω (dashed-line) and at 2ω (solid-line) as functions of the waveguide ridge width W (see Fig. 1). From the figure, the simulated birefringence at 2ω is less than an order of magnitudes smaller than that of the pump for the entire simulated values of W. Moreover, there exists a waveguide design for which the polarization degeneracy condition can be fulfilled. The small modal birefringence in addition to the existence of polarization degenerate design is a unique characteristic of Bragg reflection waveguides which deserve further

#124649 - $15.00 USD Received 24 Feb 2010; revised 23 May 2010; accepted 26 May 2010; published 28 May 2010

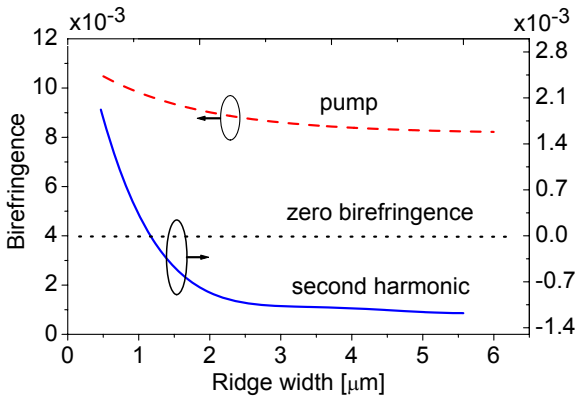

Fig. 4. Modal birefringence of pump (solid-line) and second-harmonic (dashed-line) as functions of the waveguide ridge width. The crossing point between the modal birefringence of SH with the zero birefringence (dotted-line) indicates a design for which the SH mode is polarization degenerate.

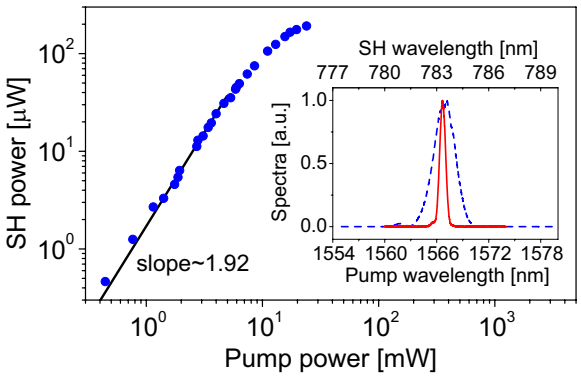

Fig. 5. Second-harmonic power as a function of pump plotted on a log-log scale. (Inset) Normalized spectra of pump (dashed-line) and SH (solid-line) obtained for the pump power of 3.3 mW.

investigation and can find potential applications involved with linear and nonlinear effects.

The quadratic dependence of SH power versus pump power was examined. The result is illustrated in Fig. 5 where the two powers are plotted on a log-log scale at the phase-matching wavelength of 1567.8 nm. Peak second-harmonic power of $\approx 190\ \mu$W was estimated for an internal pump power of ≈ 24 mW. This SH power level was comparable with that estimated in highly efficient form birefringence devices previously reported in [15]. At pump power levels below 10 mW the slope of a linear fit (solid-line) was obtained to be 1.92. For pump power above 10 mW clear deviation from a perfect quadratic dependence can be observed which were solely ascribed to third-order nonlinear effects mainly two-photon absorption. The inset of Fig. 5 shows a comparative illustration of the normalized spectra of the pump and that of the SH. The full-width at half-maximum bandwidth (FWHM) of the pump was measured as 2.4 nm, while that of the SH was 0.4 nm.

#124649 - $15.00 USD Received 24 Feb 2010; revised 23 May 2010; accepted 26 May 2010; published 28 May 2010

4. Summary

In summary, we have reported type-0 phase-matching process in *z*-grown $Al_xGa_{1-x}As$ Bragg reflection waveguide where TM_ω polarized pump was used for generating $TM_{2\omega}$ polarized second-harmonic. The interaction was essential for TM-polarized pump, where the non-vanishing pump electric field along the propagation direction initiated the nonlinear interaction. The normalized parametric conversion efficiency was estimated as 2.84×10^3 $\%W^{-1}cm^{-2}$. Also, it was demonstrated that type-I $TE_\omega \rightarrow TM_{2\omega}$ and type-II $TE_\omega + TM_\omega \rightarrow TE_{2\omega}$ processes were existed in the same waveguide. The phase-matching wavelength of all three interactions were shown to reside within a spectral range as small as 17 nm with comparable conversion efficiencies that were amongst the highest reported values in monolithic semiconductor waveguides. This has the potential to usher the way for monolithic photonic devices for non-classical and quantum optical applications helping move them into practical domains.

Acknowledgments

The authors are thankful to J. S. Aitchison for the pulse characterization setup as well as S. J. Wagner and D. C. Hutchings for informative discussions. This work was supported by the Natural Sciences and Engineering Research Council of Canada (NSERC), Ontario Centres of Excellence (OCE) and Canadian Microelectronics Corporation (CMC).

#124649 - $15.00 USD Received 24 Feb 2010; revised 23 May 2010; accepted 26 May 2010; published 28 May 2010